J|A|C|S
ARTICLES

Published on Web 07/15/2008

Thermal Signature of Hydrophobic Hydration Dynamics

Johan Qvist and Bertil Halle*

Department of Biophysical Chemistry, Center for Molecular Protein Science, Lund University, SE-22100 Lund, Sweden

Received April 17, 2008; E-mail: bertil.halle@bpc.lu.se

Abstract: Hydrophobic hydration, the perturbation of the aqueous solvent near an apolar solute or interface, is a fundamental ingredient in many chemical and biological processes. Both bulk water and aqueous solutions of apolar solutes behave anomalously at low temperatures for reasons that are not fully understood. Here, we use ^{2}H NMR relaxation to characterize the rotational dynamics in hydrophobic hydration shells over a wide temperature range, extending down to 243 K. We examine four partly hydrophobic solutes: the peptides *N*-acetyl-glycine-*N*′-methylamide and *N*-acetyl-leucine-*N*′-methylamide, and the osmolytes trimethylamine *N*-oxide and tetramethylurea. For all four solutes, we find that water rotates with lower activation energy in the hydration shell than in bulk water below 255 ± 2 K. At still lower temperatures, water rotation is predicted to be faster in the shell than in bulk. We rationalize this behavior in terms of the geometric constraints imposed by the solute. These findings reverse the classical "iceberg" view of hydrophobic hydration by indicating that hydrophobic hydration water is less ice-like than bulk water. Our results also challenge the "structural temperature" concept. The two investigated osmolytes have opposite effects on protein stability but have virtually the same effect on water dynamics, suggesting that they do not act indirectly via solvent perturbations. The NMR-derived picture of hydrophobic hydration dynamics differs substantially from views emerging from recent quasielastic neutron scattering and pump−probe infrared spectroscopy studies of the same solutes. We discuss the possible reasons for these discrepancies.

1. Introduction

As a result of the small size and multiple hydrogen-bonding capacity of the water molecule, the cohesive energy density of liquid water is an order of magnitude larger than that of most organic liquids. When an apolar solute is inserted into water, there is thus a strong tendency to maintain the dense hydrogen-bond network in the surrounding solvent. On the other hand, the high energy density of water also means that even small structural perturbations in the hydration shell can have profound thermodynamic consequences. The large negative hydration entropy of apolar solutes and its strong temperature dependence (associated with the anomalous solubility minimum) is generally attributed to the constraints imposed by the apolar solute on the orientations and positions of the adjacent, mutually hydrogen bonded, water molecules.[1–4] But neutron diffraction[5–7] and molecular simulations[8–10] show that the structural perturbations in the hydration shell are more subtle than suggested by a literal interpretation of the classical "iceberg" metaphor.[11] To a first approximation, the hydrogen-bonded water structure seems to be the same in the hydrophobic hydration shell as in the bulk solvent.

Whereas the subtle structural changes in the hydrophobic hydration shell may escape experimental detection, the sizable *dynamical* perturbations are readily characterized quantitatively. Among the available dynamical observables, the single-molecule rotational correlation time τ is a particularly useful probe of the hydration shell because of its strong dependence on the local hydrogen-bond configuration. In bulk water, molecular rotation occurs by a concerted mechanism where hydrogen bonds are simultaneously broken and reformed.[12] As a result, molecular rotation in liquid water is 6 orders of magnitude faster than in ice I_h,[13] although still a factor ∼20 slower than in the absence of hydrogen bonds.[14,15] Given the high cohesive energy density of water, one expects solute-induced structural and dynamical perturbations to be short-ranged, essentially confined to the first hydration shell. This expectation has been amply confirmed by experiment[16,17] and simulation.[8,18,19] We can therefore use a

(1) Blokzijl, W.; Engberts, J. B. F. N. *Angew. Chem., Int. Ed.* **1993**, *32*, 1545–1579.
(2) Southall, N. T.; Dill, K. A.; Haymet, A. D. J. *J. Phys. Chem. B* **2002**, *106*, 521–533.
(3) Chandler, D. *Nature* **2005**, *437*, 640–647.
(4) Ashbaugh, H. S.; Pratt, L. R. *Rev. Mod. Phys.* **2006**, *78*, 159–178.
(5) Bowron, D. T.; Soper, A. K.; Finney, J. L. *J. Chem. Phys.* **2001**, *114*, 6203–6219.
(6) Dixit, S.; Soper, A. K.; Finney, J. L.; Crain, J. *Europhys. Lett.* **2002**, *59*, 377–383.
(7) Buchanan, P.; Aldiwan, N.; Soper, A. K.; Creek, J. L.; Koh, C. A. *Chem. Phys. Lett.* **2005**, *415*, 89–93.
(8) Rossky, P. J.; Karplus, M. *J. Am. Chem. Soc.* **1979**, *101*, 1913–1937.
(9) Meng, E. C.; Kollman, P. A. *J. Phys. Chem.* **1996**, *100*, 11460–11470.
(10) Fidler, J.; Rodger, P. M. *J. Phys. Chem. B* **1999**, *103*, 7695–7703.
(11) Frank, H. S.; Evans, M. W. *J. Chem. Phys.* **1945**, *13*, 507–532.
(12) Laage, D.; Hynes, J. T. *Science* **2006**, *311*, 832–835.
(13) Petrenko, V. F.; Whitworth, R. W. *Physics of Ice*; Oxford University Press: Oxford, 1999.
(14) Nakahara, M.; Wakai, C.; Yoshimoto, Y.; Matubayasi, N. *J. Phys. Chem.* **1996**, *100*, 1345–1349.
(15) Goodnough, J. A.; Goodrich, L.; Farrar, T. C. *J. Phys. Chem. A* **2007**, *111*, 6146–6150.
(16) Woessner, D. E. *J. Magn. Reson.* **1980**, *39*, 297–308.
(17) Carlström, G.; Halle, B. *Langmuir* **1988**, *4*, 1346–1352.
(18) Vaisman, I. I.; Brown, F. K.; Tropsha, A. *J. Phys. Chem.* **1994**, *98*, 5559–5564.

two-state description of a dilute solution, where water molecules are either perturbed (in the first hydration shell) or unperturbed (bulk water beyond the first shell). Given this approximation, the mean rotational correlation time $\langle\tau_H\rangle$ for the water molecules in the first hydration shell can be determined in a model-independent way from the linear variation with solute concentration of the water ^2H or ^{17}O NMR relaxation rate. This approach has been applied to dilute aqueous solutions of a wide range of solutes with apolar groups,[14,20–33] usually at 298 K.

The correlation time $\langle\tau_H\rangle$ obtained from such NMR experiments is an average over all water molecules in the hydration shell of the solute, which, for solubility reasons, usually has polar as well as apolar parts. At 298 K, it is generally found that $\langle\tau_H\rangle$ exceeds the bulk-water correlation time τ_0, but not by more than a factor 2.[14,20–33] From the variation of $\langle\tau_H\rangle$ within a homologous series of solutes, it has been established that the retardation of water rotation is produced mainly by apolar groups, whereas amide groups have little or no effect. Thus, for urea[24,31,32,34,35] and formamide,[24] there is no significant dynamic perturbation. Molecular dynamics (MD) simulations[8,10,36–38] agree qualitatively with these NMR results. Moreover, by correlating water rotation with hydrogen-bond geometry and energetics, simulations can provide mechanistic insights that cannot be obtained from experiments. The slowing down of water rotation in the hydration shell of apolar groups thus appears to be due not to stronger water−water hydrogen bonds but to interference with the cooperative rotation mechanism that prevails in bulk water.[8,36,38,39]

Few NMR studies have examined the temperature dependence of hydrophobic hydration dynamics[14,25–27,29–31] and only one at subzero temperatures.[25] (Variable-temperature NMR studies of more concentrated solutions of alcohols[40,41] and tetraalkylammonium salts[42,43] have been reported, in the latter case extending down to 180 K.) In general, it has been found that hydrophobic hydration water rotates with a higher activation energy than bulk water,[14,29,30] and it has been suggested, on the basis of MD simulations of a krypton-like solute[36] and NMR studies of benzene solutions,[14] that hydrophobic hydration dynamics corresponds to bulk-water dynamics at a temperature reduced by 10−20 K. If this were the case, the dynamic perturbation factor $\langle\tau_H\rangle/\tau_0$ would increase monotonically on cooling. But if the rotation mechanism differs between hydration shell and bulk, as seems to be the case, this corresponding states picture may not hold over an extended temperature range.

The bulk-water rotational correlation time τ_0 increases dramatically in the supercooled regime.[44,45] Although not fully understood,[46–48] the anomalous thermal behavior of supercooled water is usually linked to subtle structural changes toward more open configurations with higher tetrahedral order at lower temperatures. In the constrained environment of the hydrophobic hydration shell, such structural changes may not be possible. It is conceivable, therefore, that the activation energy of hydrophobic hydration water crosses the bulk-water activation energy at some temperature in the supercooled regime and that hydration water actually rotates faster than bulk water at sufficiently low temperatures.

To address these issues, we have used ^2H NMR relaxation to determine $\langle\tau_H\rangle$ for four partly hydrophobic solutes in D_2O over a 65 K temperature interval extending down to 243 K. These data fill a significant gap in the experimental characterization of hydrophobic hydration dynamics. In addition, this study was motivated by the need for small-molecule reference data in studies of protein hydration at low temperatures.[49] For this reason, two of our solutes are blocked amino acids, *N*-acetyl-glycine-*N*′-methylamide (NAGMA) and *N*-acetyl-leucine-*N*′-methylamide (NALMA), the hydration dynamics of which have also been studied by quasielastic neutron scattering.[50–53] In addition, we have examined two predominantly hydrophobic osmolytes, trimethylamine *N*-oxide (TMAO) and tetramethylurea (TMU), both of which have also been investigated by polarized pump−probe IR spectroscopy.[54,55] A further objective of the present study is to critically compare the results obtained by these three techniques. The two osmolytes examined here are not only excellent hydrophobic model solutes but also of biological interest. TMU is one of the most potent protein

(19) Paschek, D. *J. Chem. Phys.* **2004**, *120*, 10605–10617.
(20) Fister, F.; Hertz, H. G. *Ber. Bunsen-Ges. Phys. Chem.* **1967**, *71*, 1032–1040.
(21) Goldammer, E. v.; Hertz, H. G. *J. Phys. Chem.* **1970**, *74*, 3734–3755.
(22) Ishimura, M.; Uedaira, H. *Bull. Chem. Soc. Jpn.* **1990**, *63*, 1–5.
(23) Shimizu, A.; Taniguchi, Y. *Bull. Chem. Soc. Jpn.* **1990**, *63*, 3255–3259.
(24) Bagno, A.; Lovato, G.; Scorrano, G.; Wijnen, J. W. *J. Phys. Chem.* **1993**, *97*, 4601–4607.
(25) Nakahara, M.; Yoshimoto, Y. *J. Phys. Chem.* **1995**, *99*, 10698–10700.
(26) Haselmeier, R.; Holz, M.; Marbach, W.; Weingärtner, H. *J. Phys. Chem.* **1995**, *99*, 2243–2246.
(27) Weingärtner, H.; Haselmeier, R.; Holz, M. *J. Phys. Chem.* **1996**, *100*, 1303–1308.
(28) Seto, T.; Mashimo, T.; Yoshiya, I.; Shimizu, A.; Fumino, K.; Taniguchi, Y. *J. Mol. Liq.* **1996**, *70*, 1–9.
(29) Ishihara, Y.; Okouchi, S.; Uedaira, H. *J. Chem. Soc., Faraday Trans.* **1997**, *93*, 3337–3342.
(30) Fumino, K.; Yukiyasu, K.; Shimizu, A.; Taniguchi, Y. *J. Mol. Liq.* **1998**, *75*, 1–12.
(31) Yoshida, S.; Ibuki, K.; Ueno, M. *J. Chem. Phys.* **1998**, *108*, 1360–1367.
(32) Shimizu, A.; Fumino, K.; Yukiyasu, K.; Taniguchi, Y. *J. Mol. Liq.* **2000**, *85*, 269–278.
(33) Okouchi, S.; Tsuchida, K.; Yoshida, S.; Ishihara, Y.; Ikeda, S.; Uedaira, H. *Bull. Chem. Soc. Jpn.* **2005**, *78*, 424–429.
(34) Finer, E. G.; Franks, F.; Tait, M. J. *J. Am. Chem. Soc.* **1972**, *94*, 4424–4429.
(35) Modig, K.; Kurian, E.; Prendergast, F. G.; Halle, B. *Protein Sci.* **2003**, *12*, 2768–2781.
(36) Zichi, D. A.; Rossky, P. J. *J. Chem. Phys.* **1986**, *84*, 2814–2822.
(37) Kalko, S. G.; Guàrdia, E.; Padró, J. A. *J. Phys. Chem. B* **1999**, *103*, 3935–3941.
(38) Xu, H.; Berne, B. J. *J. Phys. Chem. B* **2001**, *105*, 11929–11932.
(39) Sciortino, F.; Geiger, A.; Stanley, H. E. *Nature* **1991**, *354*, 218–221.
(40) Ludwig, R. *Chem. Phys.* **1995**, *195*, 329–337.
(41) Yoshida, S.; Kitajo, A.; Yamaguchi, T. *J. Mol. Liq.* **2006**, *125*, 158–163.
(42) Bradl, S.; Lang, E. W. *J. Phys. Chem.* **1993**, *97*, 10463–10471.
(43) Liegl, B.; Bradl, S.; Schätz, T.; Lang, E. W. *J. Phys. Chem.* **1996**, *100*, 897–904.
(44) Hindman, J. C. *J. Chem. Phys.* **1974**, *60*, 4488–4496.
(45) Lang, E. W.; Lüdemann, H.-D. *Angew. Chem., Int. Ed. Engl.* **1982**, *21*, 315–329.
(46) Debenedetti, P. G. *J. Phys.: Condens. Matter* **2003**, *15*, R1669–R1726.
(47) Sciortino, F.; Gallo, P.; Tartaglia, P.; Chen, S.-H. *Phys. Rev. E* **1996**, *54*, 6331–6343.
(48) Angell, C. A. *Science* **2008**, *319*, 582–587.
(49) Mattea, C.; Qvist, J.; Halle, B. *Biophys. J.* **2008**, published online June 27, doi 10.1529/biophysj.108.135194.
(50) Russo, D.; Hura, G.; Head-Gordon, T. *Biophys. J.* **2004**, *86*, 1852–1862.
(51) Russo, D.; Murarka, R. K.; Hura, G.; Verschell, E.; Copley, J. R. D.; Head-Gordon, T. *J. Phys. Chem. B* **2004**, *108*, 19885–19893.
(52) Russo, D.; Murarka, R. K.; Copley, J. R. D.; Head-Gordon, T. *J. Phys. Chem. B* **2005**, *109*, 12966–12975.
(53) Malardier-Jugroot, C.; Head-Gordon, T. *Phys. Chem. Chem. Phys.* **2007**, *9*, 1962–1971.
(54) Rezus, Y. L. A.; Bakker, H. J. *Phys. Rev. Lett.* **2007**, *99*, 148301.
(55) Rezus, Y. L. A.; Bakker, H. J. *J. Phys. Chem. A* **2008**, *112*, 2355–2361.

denaturants,[56] and TMAO is produced by marine organisms to counteract the destabilizing effect of urea.[57]

2. Materials and Methods

2.1. Sample Preparation. Trimethylamine *N*-oxide (TMAO, Aldrich), tetramethylurea (TMU, Aldrich), *N*-acetyl-glycine-*N*′-methylamide (NAGMA, Bachem), and *N*-acetyl-leucine-*N*′-methylamide (NALMA, Bachem) were used as supplied (>98 or 99% purity). The solutes were dissolved in D_2O (99.9 atom % ^2H, low paramagnetic content, CIL). All solutions also contained ~4 mM NaN_3, which has no significant effect on the ^2H relaxation.

Relaxation measurements at temperatures below the equilibrium freezing point of D_2O were performed on emulsion samples,[58] prepared by mixing ~1 mL of D_2O solution with an equal volume of *n*-heptane (>99%, HPLC grade, Sigma) containing 3% (w/w) of the nonionic emulsifier sorbitan tristearate (Sigma). A water-in-oil emulsion with aqueous droplet diameters in the range 1−15 μm was obtained by mixing the two solutions with the aid of two 5 mL syringes connected via a 0.56 mm i.d. nozzle (Hamilton) and pressing the mixture through the nozzle ~40 times.

Solute concentrations were kept below 0.22 M to avoid self-association, segregation, and hydration shell overlap. At higher concentrations (0.5 or 1 M), R_1 was, for all four solutes, slightly larger than expected from linear extrapolation of the low-concentration data, indicating that solute−solute interactions affect the hydration dynamics. Solute concentrations, expressed as the water/solute mole ratio N_W, were determined gravimetrically and by ^1H NMR spectroscopy, with excellent agreement (Supporting Information S1). ^1H NMR was also used to demonstrate that the solutes partition exclusively in the aqueous phase of the emulsion samples (Supporting Information S1).

The solution pH* (the pH-meter reading without isotope correction) was 4.5 for NAGMA, NALMA, and TMU. At pH* 4.5 and T < 308 K, the two labile deuteron atoms in NAGMA and NALMA exchange with water deuterons on a time scale > 10 s,[59] but since their intrinsic ^2H relaxation times are <0.1 s, these labile deuterons should not contribute significantly to the spin relaxation of the observed water ^2H magnetization. This expectation was confirmed by measuring the water ^2H and ^{17}O (at natural abundance) relaxation rates in the same sample and finding that the relative relaxation enhancements agree within experimental error (Table S2). Solution pH* was 6.8 for TMAO, well above its pK_a value of 4.66.[60] TMAO is thus present in zwitterionic form.

2.2. Water ^2H Relaxation Measurements. The relaxation rate, R_1, of the water ^2H longitudinal magnetization was measured at 55.5 MHz on a Varian Unity NMR spectrometer. Control experiments were also performed at 76.8 MHz and on the ^{17}O nuclide (Supporting Information S2). R_1 was determined with 0.5−1.0% accuracy from three-parameter fits to single-exponential inversion−recovery curves with 30 delay times. The ice signal from the small fraction of water droplets that freeze by heterogeneous nucleation at temperatures below 277 K is broadened beyond detection and does not affect the R_1 measurement. No freezing could be detected during the R_1 measurements even at 243 K. At each temperature, measurements of R_1^0 on pure D_2O reference samples were alternated with solution R_1 measurements. The samples were carefully equilibrated at each temperature, which was regulated with a precooled stream of dry air and determined before and after R_1 measurements with a copper-constantan thermocouple in an NMR tube containing a water−ethanol mixture.

2.3. Hydration Numbers. Five 1 ns MD simulations of ~35 mM solutions of the four investigated solutes were performed as described in Supporting Information S3. The simulation trajectories were used to compute the number ν_H of water molecules in the first hydration shell of each solute (Table S3). Hydration numbers for other solutes, previously studied by water ^{17}O relaxation, were computed from the solvent-accessible surface area in such a way that they are consistent with the MD-derived ν_H values for the four solutes examined here (Supporting Information S3 and Table S4).

3. Theoretical Background

The relaxation rate R_1 of the longitudinal water ^2H magnetization probes the rotational dynamics of individual water molecules via rotationally induced fluctuations of the nuclear electric quadrupole coupling.[61] In the solutions studied here, fast water diffusion averages over all solute-induced dynamical heterogeneities on a time scale that is several orders of magnitude shorter than the ^2H spin relaxation time (20−500 ms). The observed R_1 is therefore an average over all water molecules in the solution. Furthermore, even at the lowest temperature investigated here (243 K), water rotation is fast compared to the inverse resonance frequency (~3 ns). Therefore, R_1 is independent of resonance frequency (Table S2), and it can then be expressed as

$$R_1 = \omega_Q^2 \langle \tau \rangle \tag{1}$$

where ω_Q is the nuclear quadrupole frequency, defined as $(3/2)^{1/2}\,\pi\,\chi\,(1 + \eta^2/3)^{1/2}$ with χ the quadrupole coupling constant and η the asymmetry parameter of the electric field gradient tensor.[61] Further, τ is the rotational correlation time, defined as the time integral of the rank-2 orientational time correlation function.[61]

In the limit of infinite dilution, R_1 must vary linearly with solute concentration or with $1/N_W$, where N_W is the water/solute mole ratio. Typically, the linearity breaks down when N_W is of the same order as the hydration number ν_H, defined here as the number of water molecules in the first coordination shell around the solute. This is also the case for the four solutes examined here, for which we observe a significant deviation from linearity at $N_W \approx 50$ (data not shown). This observation indicates that the solute-induced perturbation of water dynamics is short-ranged, being essentially confined to the first hydration shell. This conclusion is supported by MD simulations of small solutes in water[8,18,19] and by water NMR relaxation studies of extended aqueous interfaces.[16,17] In the present study, we only use data from sufficiently dilute solutions (N_W > 250; Table S1) that overlap or interference of hydration shells can be safely ignored.

Since variations in water dynamics within the hydration shell cannot be resolved, water NMR relaxation data are usually analyzed with a two-state model. The solution-average correlation time is thus expressed as

$$\langle \tau \rangle = \left(1 - \frac{\nu_H}{N_W}\right)\tau_0 + \frac{\nu_H}{N_W}\langle \tau_H \rangle \tag{2}$$

where τ_0 is the bulk-water correlation time and $\langle \tau_H \rangle$ is the average correlation time in the hydration shell. Combination of eqs 1 and 2 yields for the relative relaxation enhancement

(56) Herskovits, T. T.; Jaillet, H.; Gadegbeku, B. *J. Biol. Chem.* **1970**, *1970*, 4544–4550.
(57) Yancey, P. H.; Clark, M. E.; Hand, S. C.; Bowlus, R. D.; Somero, G. N. *Science* **1982**, *217*, 1214–1222.
(58) Rasmussen, D. H.; MacKenzie, A. P. *J. Chem. Phys.* **1973**, *59*, 5003–5013.
(59) Bai, Y.; Milne, J. S.; Mayne, L.; Englander, S. W. *Proteins* **2004**, *17*, 75–86.
(60) Singh, R.; Haque, I.; Ahmad, F. *J. Biol. Chem.* **2005**, *280*, 11035–11042.
(61) Abragam, A. *The Principles of Nuclear Magnetism*; Clarendon Press: Oxford, 1961.

$$\frac{R_1 - R_1^0}{R_1^0} = \frac{\nu_{dyn}}{N_W} \tag{3}$$

where we have introduced the "dynamic hydration number" (DHN)

$$\nu_{dyn} = \nu_H(\xi - 1) \tag{4}$$

which involves the static (geometric) hydration number ν_H and the dynamic perturbation factor (DPF)

$$\xi = \frac{\langle \tau_H \rangle}{\tau_0} \tag{5}$$

The right-hand side of eq 3 is often expressed as $B\, m_S$, where m_S is the solute molality.[62] It follows that $B = M_W\, \nu_{dyn}$, where M_W is the molar mass of water. We prefer ν_{dyn} over B because it is dimensionless and (to first-order) the same for H_2O and D_2O (allowing direct comparison of ^{17}O and ^2H results).

The relationship between the DPF and the measured R_1 expressed by eqs 3−5 assumes that the quadrupole frequency ω_Q has the same (mean) value in the hydration shell as in bulk water. This is a good approximation because the electric field gradient at the position of the water deuterons is primarily determined by the nuclear geometry and electron distribution of the water molecule,[63,64] which are not significantly perturbed by the solute. Also the (smaller) intermolecular contribution to the field gradient is insensitive to replacement of (some of the) water−water interactions by water−solute interactions. Quantum-mechanical field-gradient calculations on configurations from MD simulations of aqueous DMSO solutions show that ω_Q is nearly invariant over the full composition range.[65] For example, in an equimolar mixture, ω_Q deviates by less than 2% from the bulk-water value.[65] Similarly, in the solid clathrate hydrate of tetrahydrofuran (THF·17D_2O), ω_Q is within 1% of the value for ice I_h.[66] For bulk D_2O, both experimental and theoretical results indicate that ω_Q is virtually independent of temperature in the range 260−370 K.[64] Given the small effect of the solute, this should also be the case for hydration water, justifying our neglect of any difference in ω_Q between hydration shell and bulk solvent at the investigated temperatures.

The DHN is an average over all water molecules in the hydration shell and therefore does not reveal the perturbing effect of the different chemical groups in a multifunctional solute. However, the DHN can be dissected by systematic variation of the solute structure. Whereas a strict group additivity is neither expected nor observed, two striking results have emerged from previous studies. First, the amide group has no significant effect on hydration dynamics, with $\nu_{dyn} = 0$ for formamide[24] and urea.[24,31,32,34,35] Second, apolar groups are more effective than polar groups in slowing down hydration water dynamics.[22–24,28–33] These regularities are illustrated in Figure 1, where the DHN for 40 organic solutes (Table S4), including the four studied here, is shown to correlate strongly ($r = 0.95$) with the number of sp^3 carbon atoms (that is, not counting carbonyl carbons). The regression line is $\nu_{dyn} = (-0.066 \pm 0.002) + (4.39 \pm 0.04)n_C$. Similar correlations have been noted previously for smaller sets of homologous solutes.[32]

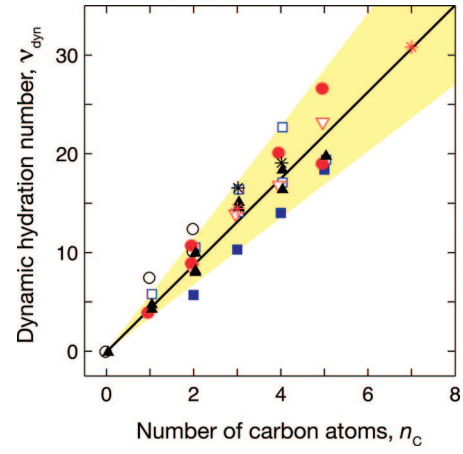

Figure 1. Dynamic hydration number, ν_{dyn}, at 298 K versus number of sp^3 carbon atoms, n_C, in 40 organic solutes, including 7 primary alcohols[29] (□), 4 diols[29] (■), 4 amino alcohols[33] (red ∇), 11 alkyl amides[24] (▲), 5 alkyl ureas[32] (○, ∗), TMAO (∗), 5 amino acids[22] (●), and 3 dipeptides[22] (●, ∗). The solutes studied here are labeled with red (NAGMA, NALMA) or black (TMAO, TMU ∗). At the extremes are urea and formamide ($n_C = 0$) and NALMA ($n_C = 8$). To reduce overlap, some data symbols have been placed slightly off the integral n_C values. The line resulted from a fit to the 40 data points and the yellow area is bounded by lines with a 30% larger or smaller slope.

Part of the correlation seen in Figure 1 is a trivial size effect (via ν_H), but this is not the whole story. Whereas only a modest correlation ($r = 0.71$) is found between ν_{dyn} and the total number of non-hydrogen atoms, a more respectable correlation ($r = 0.86$) exists between $\xi - 1$ and n_C for these 40 solutes (Table S4). The four solutes examined here have 3−8 sp^3 carbons, and we therefore expect that ν_{dyn} reports mainly on water dynamics in the hydrophobic part of the hydration shell.

From the temperature dependence of the DHN, we can obtain the activation energy for water rotation in the hydration shell. Taking the static hydration number ν_H to be independent of temperature, we obtain, from eqs 4 and 5,

$$\frac{d\nu_{dyn}}{dT} = \frac{\nu_H \xi(T)}{k_B T^2}\left[E_A^0(T) - E_A^H(T)\right] \tag{6}$$

where $E_A^H(T)$ is the apparent Arrhenius activation energy for the hydration shell, defined through

$$E_A^H(T) = -k_B T^2 \frac{d \ln\langle \tau_H \rangle}{dT} \tag{7}$$

and similarly for bulk water. In the few previous variable-temperature studies,[14,29–31] the DHN was found to increase on cooling, $d\nu_{dyn}/dT < 0$, implying a larger activation energy in the hydration shell than in bulk water. However, at the lower temperatures accessed here, we find that the DHN exhibits a maximum at a crossover temperature T_X, defined by

$$E_A^0(T_X) = E_A^H(T_X) \tag{8}$$

4. Results

For each of the four solutes, we have determined the DHN at 10 temperatures in the range 243−308 K from the dependence of the water ^2H relaxation rate R_1 on solute concentration. At the five lowest temperatures, the aqueous solution is in a

(62) Bagno, A.; Rastrelli, F.; Saielli, G. *Prog. Nucl. Magn. Reson. Spectrosc.* **2005**, *47*, 41–93.
(63) Eggenberger, R.; Gerber, S.; Huber, H.; Searles, D.; Welker, M. *J. Chem. Phys.* **1992**, *97*, 5898–5904.
(64) Ludwig, R.; Weinhold, F.; Farrar, T. C. *J. Chem. Phys.* **1995**, *103*, 6941–6950.
(65) Müller, M. G.; Hardy, E. H.; Vogt, P. S.; Bratschi, C.; Kirchner, B.; Huber, H.; Searles, D. J. *J. Am. Chem. Soc.* **2004**, *126*, 4704–4710.
(66) Davidson, D. W.; Garg, S. K.; Ripmeester, J. A. *J. Magn. Reson.* **1978**, *31*, 399–410.

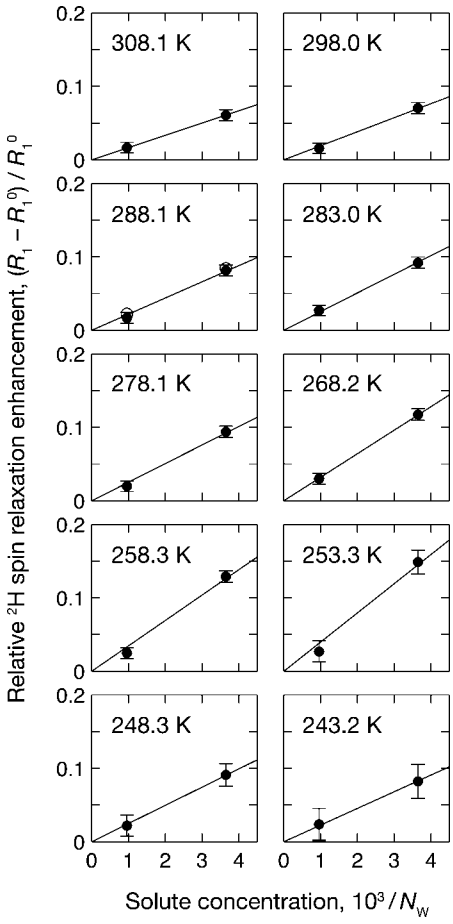

Figure 2. Relative ^{2}H spin relaxation enhancement versus TMU concentration, measured on solution (five highest temperatures) or emulsion (five lowest temperatures) samples. At 288.1 K, results from emulsion (●) and solution (○) samples are compared. The regression lines were forced to pass through the origin.

metastable supercooled state below its equilibrium freezing temperature. To access as low a temperature as possible, the aqueous solution was dispersed as ~10 μm droplets in a water-in-oil emulsion (Materials and Methods). Several control experiments were performed, demonstrating that the emulsion has no significant effect on R_1. To ensure that the water molecules in the sample are dynamically perturbed by at most one solute molecule at a time, the highest solute concentration used was 0.22 M (Table S1). Even at such low concentrations, the relative relaxation enhancement $(R_1 - R_1^0)/R_1^0$ is an order of magnitude larger than the relative experimental error in R_1.

As predicted by eq 1, the relative relaxation enhancement was found to be proportional to $1/N_W$ in the low-concentration regime. This is illustrated for TMU in Figure 2. The DHN, which is given by the slope of the fitted lines, is seen to exhibit a maximum as a function of temperature. The temperature dependence of the DHN obtained in this way is shown in Figure 3 for each of the four solutes. A DPF maximum is clearly evident for NALMA and TMU.

The static hydration number ν_H, that is, the number of water molecules in the first hydration shell, was determined from MD simulations (Table 1, Supporting Information S3). Using eq 4, we thus obtained the dynamic perturbation factor ξ. The bulk-water correlation time τ_0 shown in Figure 3 was obtained from eq 1, with the ^{2}H relaxation rate R_1^0 measured on pure D_2O reference samples and the known ^{2}H quadrupole frequency $\omega_Q = 1.02 \times 10^6$ s^{-1}.[64] By inserting $\tau_0(T)$ and $\xi(T)$ into eq 5, we obtained the mean hydration-shell correlation time $\langle\tau_H\rangle$ shown in Figure 3. For all four solutes, it is evident that $\langle\tau_H\rangle$ has a weaker temperature dependence than τ_0 at the low-temperature end of the investigated range. This means that the apparent activation energy E_A^H is smaller than E_A^0 and that ν_{dyn} decreases on cooling at these low temperatures. Although a DHN maximum is only evident in the measured ν_{dyn} data for NALMA and TMU, we can predict the behavior of $\nu_{dyn}(T)$ at the lowest temperature (where accurate R_1 measurements for NAGMA and TMU could not be obtained) by extrapolating the monotonic and smooth temperature dependence of $\langle\tau_H\rangle$. As found previously,[45] the temperature dependence of τ_0 is accurately described by a power law: $\tau_0(T) = A(T/T_C - 1)^{-\gamma}$ (blue curves in Figure 3). The weaker temperature dependence of $\langle\tau_H\rangle$ was represented by a three-parameter rational fraction: $\langle\tau_H(T)\rangle = (a + bT)/(1 + cT)$ (red curves in Figure 3). The $\nu_{dyn}(T)$ curves in Figure 3, which all exhibit maxima, were obtained from eqs 4 and 5 and these numerical representations of the temperature-dependent τ_0 and $\langle\tau_H\rangle$.

Table 1 presents DHN and DPF values at 298 K and at the crossover temperature T_X (where the DHN and DPF have maxima) obtained from the fitted $\nu_{dyn}(T)$ curves in Figure 3. As generally found for organic solutes (Table S4), the room-temperature DPF is in the range 1−2 also for these four solutes and, as expected from the general correlation with hydrophobicity (Figure 1), the DPF is smallest for the least hydrophobic solute NAGMA. At room temperature, water rotation in the hydration shell is thus slowed down by less than a factor of 2 as compared to bulk water. Even at the maximum, the largest DPF is only 2.4 (for NALMA). As seen from Figure 3, the predicted zero-crossing of the DHN is at 237 ± 1 K for these four solutes. At lower temperatures, we thus expect that $\xi < 1$; that is, water rotation would be faster in the hydration shell than in the bulk liquid.

For all four solutes, the crossover temperature T_X, where $E_A^H = E_A^0$, lies in the narrow range 253−257 K. At lower temperatures, the apparent activation energy for water rotation is smaller in the hydration shell than in the bulk liquid. This crossover phenomenon is illustrated in Figure 4, where we also compare our data with the previously published temperature-dependent water relaxation data for benzene[25] and primary alcohols.[29] At higher temperatures (>270 K), the activation energy is larger in the hydration shell than in bulk water and it is largest for the most hydrophobic solutes. For benzene, with the highest activation energy, no DHN maximum was observed[14,25] (the lowest examined temperature was 255 K), but the (extrapolated) crossover temperature is only slightly lower (T_X = 251.4 K) than that for the four solutes examined here. It should be noted that the benzene results were derived from measurements at a single solute concentration (23 mM), the solubility limit at 295 K.[25] The interpretation of the low-temperature behavior thus relies on the assumption that the solubility of benzene in D_2O does not decrease on cooling.

5. Discussion

5.1. Interpretation of the Crossover Phenomenon. The present study extends the existing rather comprehensive knowledge base on the hydration dynamics of organic solutes at room temperature (Table S4) by monitoring the hydration dynamics of four biologically relevant solutes over a wide temperature range. Our results reveal a hitherto unknown crossover phenomenon at a

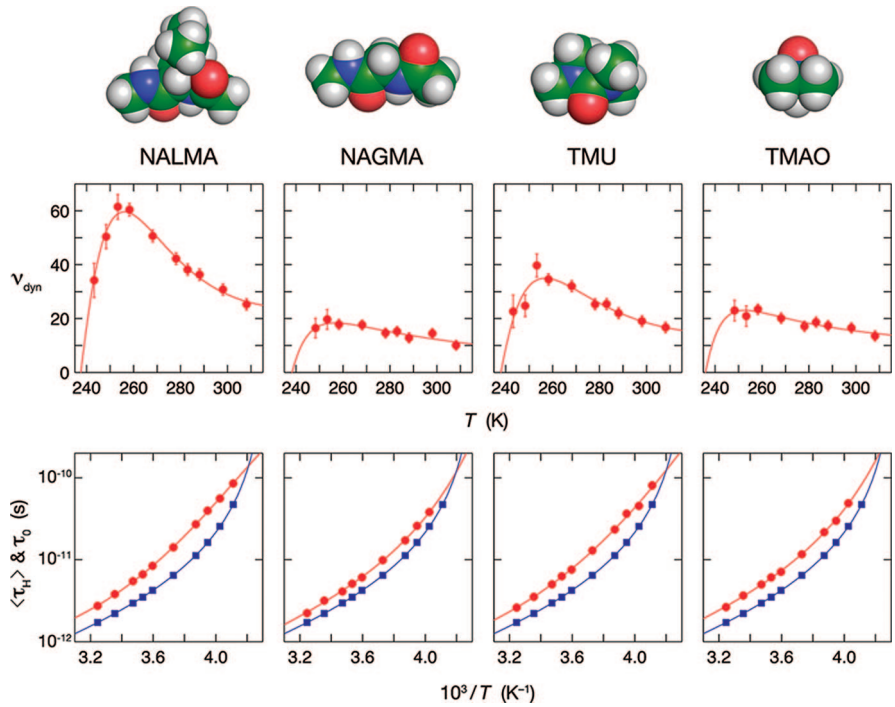

Figure 3. (Upper panels) Temperature dependence of the dynamic hydration number ν_{dyn} for the four solutes depicted at the top. The curves were constructed from fits to τ_0 and $\langle\tau_H\rangle$. (Lower panels) Arrhenius plots of the temperature dependence of the bulk water correlation time τ_0 (■) and the mean hydration-shell correlation time $\langle\tau_H\rangle$ (●). The fitted curves were obtained as described in the text.

Table 1. DHN and DPF at 298 K and at T_X for Four Solutes

property	NAGMA	NALMA	TMAO	TMU
ν_H[a]	33.3 ± 2.6	42.6 ± 2.8	25.1 ± 2.0	32.0 ± 2.4
ν_{dyn}(298 K)	12.5	29.7	15.6	19.0
ξ(298 K)	1.37	1.70	1.62	1.59
T_X (K)	256.6	256.0	256.9	252.8
$\nu_{dyn}(T_X)$	18.4	59.6	23.0	35.0
$\xi(T_X)$	1.55	2.40	1.92	2.09

[a] Mean and standard deviation calculated from 1 ns MD trajectory.

temperature $T_X = 255 \pm 2$ K, below which the apparent activation energy for water rotation is smaller in the hydration shell than in bulk water. At higher temperatures, the activation energy is larger in the hydration shell, but on cooling, it increases less strongly than it does in bulk water. In bulk water, the apparent activation energy increases on cooling because the liquid structure is gradually transformed toward more open configurations with higher tetrahedral order. In the hydration shell of a hydrophobic solute or residue, the solute's inability to participate in the aqueous H-bond network imposes orientational constraints that limit the configurational freedom of the adjacent water molecules. While the hydration structure becomes more ordered on cooling, accounting for the increased activation energy, the ice-like configurations that presumably are responsible for the strong temperature-dependence in supercooled bulk water cannot form in the hydration layer. The view that emerges from this interpretation of the observed crossover phenomenon reverses the classical "iceberg" view of hydrophobic hydration. At least at low temperatures, the bulk solvent is more ice-like than the hydration shell. (The term "ice-like" refers to structure; even at 243 K the rotational dynamics in bulk water is 4 orders of magnitude faster than that in ice I_h.)

5.2. Comparison with Results Obtained by QENS. The hydration dynamics of NAGMA and NALMA have previously been studied by QENS and MD simulations.[50–52] These studies were performed at or above the concentrations (1.0 M NAGMA and 0.5 M NALMA) where we find that R_1 no longer depends linearly on solute concentration. The QENS and MD results may therefore differ from our results, which pertain to the hydration shell of the "isolated" solute. For a 1.0 M NALMA solution (where the total water content, $N_W = 45.9$, is similar to the primary hydration number, $\nu_H = 42.6$), QENS data acquired in the temperature range 248−288 K gave rotational correlation times in the range 1.8−3.2 ps,[53] up to a factor of 4 *shorter* than the correlation time τ_0 for bulk H_2O.[45] For example, the QENS data yield $\xi = 0.24$ at 248 K where we find $\xi = 2.2$ (Figure 3). Furthermore, the QENS data yielded a temperature-independent activation energy for water rotation of 8.7 kJ mol^{-1},[53] whereas we find that E_A^H increases (on cooling) from 27.8 to 41.0 kJ mol^{-1} in this temperature interval (Figure 4). At room temperature, the 1.0 ps rotational correlation obtained from 1.0 M NAGMA and NALMA solutions was linked to "large-amplitude librational motions",[52] whereas an elastic component of the incoherent structure factor was taken as evidence for a large fraction (66% and 38%, respectively) of rotationally "immobilized" water molecules, defined as water molecules with rotational correlation times outside the QENS window (≫13 ps). This implies that $\xi \gg 5$ for NAGMA, whereas we find $\xi = 1.4$ at 298 K (Table 1).

We attribute these order-of-magnitude discrepancies between QENS and NMR results primarily to the strong model-dependence in the interpretation of the QENS data[67,68] and the limited time-scale window (1−13 ps) accessed by the QENS experiments and secondarily to the high solute concentration used in the QENS study. That the concentration difference is not the main reason for the discrepancies is suggested by the fact that MD simulations of (concentrated) NAGMA and

(67) Bée, M. *Quasielastic Neutron Scattering*; Adam Hilger: Bristol, 1988.
(68) Murarka, R. K.; Head-Gordon, T. *J. Chem. Phys.* **2007**, *126*, 215101.

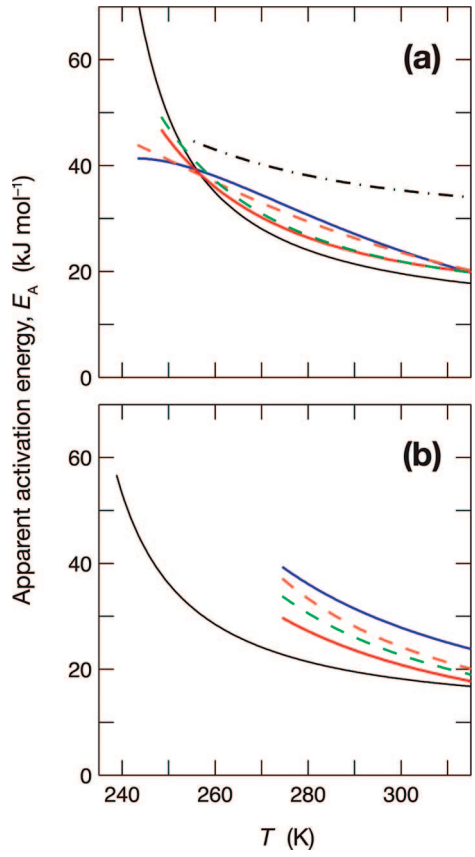

Figure 4. (a) Temperature dependence of the apparent activation energy for water rotation in bulk D_2O (black solid curve) and in the hydration shells of NAGMA (red solid), TMAO (green dashed), TMU (orange dashed), NALMA (blue solid), and benzene (black dash-dotted),[25] derived from water ^2H relaxation data. (b) Temperature dependence of the apparent activation energy for water rotation in bulk H_2O (black solid curve) and in the hydration shells of methanol (red solid), ethanol (green dashed), *n*-propanol (orange dashed), and *tert*-butanol (blue solid), derived from water ^{17}O relaxation data on emulsified H_2O (J. Qvist, C. Mattea, B. Halle, to be published) and on aqueous alcohol solutions.[29]

NALMA solutions[68] yield DPFs more in line with our results. For ~1.0 M NAGMA ($N_W = 55.0$), the simulation gave $\langle\tau\rangle = 2.27$ ps and $\tau_0 = 1.90$ ps. Using eqs 2 and 5 with $\nu_H = 33.3$ (Table 1), we find that this corresponds to $\xi = 1.32$, not far from our (dilute solution) result $\xi = 1.37$ (Table 1). Similarly, for ~0.5 M NALMA ($N_W = 92.4$), the simulation data yield $\xi = 1.46$ while we find $\xi = 1.70$ (Table 1).

5.3. Comparison with Results Obtained by Pump−Probe IR Spectroscopy. The other two solutes examined here, TMAO and TMU, have recently been investigated by polarized pump−probe IR spectroscopy.[54,55] This technique shares two of the limitations of QENS: the need for high solute concentrations (for sensitivity reasons) and a restricted (<10 ps) experimental time-scale window (because of vibrational relaxation). The principal conclusion of the IR study was that 6.0 (TMAO) or 7.4 (TMU) water molecules in the hydration shell (that is, ~2 per methyl group) are "strongly immobilized", meaning that the rotational correlation time is well outside the experimental window (≫10 ps) at room temperature, while the remaining (~20) water molecules in the hydration shell are essentially unperturbed.[54,55] This result was taken to support a literal interpretation of the "iceberg" metaphor.[11] If this interpretation is correct, the hydration-shell correlation time determined by NMR can be expressed as

$$\langle\tau_H\rangle = (1 - f_s)\tau_{Hf} + f_s\tau_{Hs} \quad (9)$$

where f_s is the fraction of slow water molecules in the hydration shell. For TMAO at 298 K, we find $\xi = 1.62$, and with $\tau_0 = 2.5$ ps from IR measurements on bulk water,[69] eq 5 yields $\langle\tau_H\rangle = 4.05$ ps. According to the IR results for TMAO, $f_s = 7.4/32 = 0.23$ and $\tau_{Hf} = \tau_0$ so eq 9 yields $\tau_{Hs} = 9.2$ ps. This means that 66% of the slow component of the anisotropy function has decayed after 10 ps, whereas the author's interpretation requires the slow component to be static on this time scale ($\tau_{Hs} \gg 10$ ps).

To resolve this discrepancy, we propose a different interpretation of the IR data. The existence of "immobilized" water molecules in the hydration shell is inferred from the observation that the anisotropy function $R(t)$ does not decay to zero in the experimental 10 ps window but appears to level out at a constant value. However, the plateau need not be associated with a subset of slowly rotating water molecules. More likely, it reflects a slow component in the orientational relaxation of all (or most) water molecules in the hydration shell. In this interpretation,

$$R(t) = \frac{2}{5}\{(1-p)\exp(-t/\tau_0) + p[(1-S^2)\exp(-t/\tau_H^f) + S^2\exp(-t/\tau_H^s)]\} \quad (10)$$

where $p = \nu_H/N_W$ is the fraction of water in the hydration shell, S is an orientational order parameter, and τ_H^f and τ_H^s are correlation times describing the fast and slow orientational relaxation steps. At low solute concentrations, $S^2 \ll 1$ so the last term in eq 10 can be neglected. The quantity measured by NMR is the time integral of the expression within curly brackets, which then coincides with eq 2. From measurements on dilute TMAO solutions at 298 K, we obtain $\xi = \tau_H^f/\tau_0 = 1.62$ (Table 1). Because τ_H^f is so close to τ_0, the biexponentiality in $R(t)$ cannot be resolved. Indeed, the $R(t)$ data for 1 M TMAO ($N_W = 55.5$) are well described by a single exponential with $\langle\tau\rangle = 2.86 \pm 0.03$ ps. This effective correlation time can be interpreted according to eq 2, and with $\nu_H = 25$ (Table 1) and $\tau_0 = 2.5$ ps,[69] we then find $\xi = 1.32$, slightly below the NMR result. At high TMAO concentrations, water molecules are confined between solute molecules and therefore experience an anisotropic environment that relaxes on the longer time scale $\tau_H^s \gg 10$ ps. For example, the $R(t)$ data at 4 M TMAO ($N_W = 13.9$ and thus $p = 1$) are well described by eq 10 with $\tau_H^f = 2.5 \pm 0.2$ ps and $S^2 = 0.37 \pm 0.05$ (and $\tau_H^s \gg 10$ ps). This interpretation obviates the need to explain why two of the ~10 water molecules that coordinate a methyl group should rotate an order of magnitude slower than the others (and continue to do so when $N_W = 9$).

The same technique was used to infer the existence of two types of hydration water in urea solutions, with 0.6 water molecules being "strongly immobilized" and the others exhibiting bulk-like dynamics.[70] In contrast, five independent NMR studies have found (at low solute concentrations) that urea has a negligible effect on the rotation of water molecules in the hydration shell.[24,31,32,34,35] The most accurate result for urea in H_2O is $\xi = 1.00 \pm 0.02$.[32] MD simulations also show that urea has little or no effect on the structure and dynamics of its hydration water.[71–73] In the IR study, the lowest urea concentra-

(69) Rezus, Y. L. A.; Bakker, H. J. *J. Chem. Phys.* **2006**, *125*, 144512.
(70) Rezus, Y. L. A.; Bakker, H. J. *Proc. Natl. Acad. Sci. U.S.A.* **2006**, *103*, 18417–18420.
(71) Kuharski, R. A.; Rossky, P. J. *J. Am. Chem. Soc.* **1984**, *106*, 5786–5793.

tion was 3.4 M, corresponding to $N_W = 13.5$, less than the primary hydration shell, $\nu_H = 20.6$ (Table 1). Even so, the $R(t)$ data[70] are well fitted by an exponential decay with $\langle\tau\rangle = 2.83 \pm 0.03$ ps, consistent with NMR results showing a considerable nonlinearity at this concentration.[35] At the very high concentration of 7.8 M ($N_W = 4.6$), the $R(t)$ data are well described by eq 10 with $\tau_0 = \tau_H^f = 2.6 \pm 0.1$ ps and $S^2 = 0.13 \pm 0.02$. Despite the very high concentration, the orientational confinement is less severe for urea (smaller S^2), which can participate in the H-bond network, than for TMAO, which cannot. Thus, as in the case of the hydrophobic solutes, there is no need to invoke "immobilized" hydration water. The $R(t)$ data can be explained by a modest orientational bias of confined water molecules, and the slow ($\gg$10 ps) process can be identified with the breakup of transient urea "cages". Such transient confinement effects should also affect QENS measurements at high solute concentrations. Indeed, MD simulations of 2 M NALMA[50] show an orientational time correlation function with the same kind of plateau as seen in the IR studies.

6. Concluding Remarks

A large number of NMR studies, including the present one, have shown that, at room temperature, water rotation in the hydration shell of an apolar solute or chemical group is slowed down by a factor 1.5−2.0 relative to bulk water (Table S1, Table S4). At lower temperatures, this dynamic perturbation factor (DPF) increases since the apparent activation energy is higher in the hydration shell than in bulk water. However, by examining the hydration dynamics in deeply supercooled solutions, we find that the DPF reaches a maximum value at the temperature T_X where the activation energy is the same in the hydration shell and in bulk water (Table 1). For the four solutes examined here, the crossover occurs at $T_X = 255 \pm 2$ K. This finding shows that hydrophobic hydration water does not simply behave as bulk water at a lower temperature. In other words, the "structural temperature" concept[74] does not capture the solute-induced perturbation.

The slower water rotation and higher activation energy is often taken as evidence for an "enhanced structure" in the hydrophobic hydration shell as compared to bulk water. Such poetic explanations may be misleading unless they are accompanied by a precise definition of water structure. Indeed, much of the confusion in the water literature stems from indiscriminate use of the word "structure". Furthermore, the connection between water dynamics and structure is nontrivial. Whereas removal of *some* of the adjacent potential hydrogen-bonding partners slows down water rotation, as seen, for example, in going from bulk water or the hydration shell of urea to the hydration shell of TMU, the removal of *all* hydrogen bonds greatly speeds up water rotation, as when water is molecularly dispersed in an apolar solvent.[14,15] Our finding that below 255 K the activation energy for water rotation in the hydrophobic hydration shell is smaller than that in bulk water suggests that the hydration shell is *less* ice-like than bulk water, thus contradicting the classical "iceberg" picture.[11]

To understand the effects of temperature and solutes on water dynamics, it must be recognized that water rotation is a highly cooperative process where large energy barriers are circumvented by a concerted interchange of hydrogen-bonding partners.[12] In bulk water, the anomalously strong (super-Arrhenius) slowing down of water rotation, particularly in the supercooled regime, is caused by interference with the cooperative rotation mechanism as the liquid structure becomes more open and tetrahedrally ordered, that is, more ice-like. In the hydrophobic hydration shell, the slowing down of water rotation, at any temperature, can also be attributed to interference with the cooperative rotation mechanism, but now the availability of new hydrogen-bonding partners is reduced by the presence of the apolar solute.[8,39] Because of the geometrical constraints imposed by the solute, the structure of the hydrophobic hydration shell changes less than the structure of bulk water as the temperature is reduced. The apparent activation energy therefore increases less in the hydration shell than in bulk water, and eventually (below 255 K) it becomes smaller in the hydration shell. In fact, our results indicate that hydrophobic hydration water rotates faster than bulk water at temperatures below 237 K.

The solutes studied here include two potent osmolytes. Despite considerable efforts, a universal molecular mechanism by which osmolytes alter the conformational stability of proteins has not been convincingly demonstrated.[75–82] The present finding that TMU (a strong protein denaturant) and TMAO (a strongly stabilizing osmolyte) perturb their hydration shells to the same extent (Table 1) supports the view that these osmolytes interact directly with the protein[75,78,79,82] rather than acting indirectly via their effect on the solvent.[77] Furthermore, since these two osmolytes are equally hydrophobic (~90% of the solvent-accessible surface area is apolar), their opposite effects on protein stability can hardly be correlated with their polarity.[79]

The hydration dynamics of the solutes examined here have also been investigated with QENS[50–53] and by pump−probe IR spectroscopy.[54,55] The resulting views of hydration dynamics differ substantially from the picture emerging from our NMR data. We identify two main reasons for this discrepancy. First, to determine the effect of a solute on water dynamics and structure, one should study the "free" hydration shell of an "isolated" solute molecule. In other words, hydration effects should be defined in terms of the rate of change induced by the solute in the limit of zero solute concentration. For sensitivity reasons, it may be challenging to work in the concentration regime where the measured effect varies linearly with solute concentration, as expected for a dilute solution with nonoverlapping hydration shells. Second, no existing experimental technique can *directly* measure the rate of water rotation in the hydration shell; a model-dependent interpretation step is always involved. The NMR relaxation method used here and elsewhere[14,20–33] is nonperturbing (e.g., there is no significant local heating, as in pump−probe laser spectroscopy) and selective (no other species than water molecules and no other motional modes than rotation influence the measurements), and it has a rigorous theoretical basis.[61] The only significant model dependence in the analysis of the NMR relaxation data presented here

(72) Åstrand, P.-O.; Wallqvist, A.; Karlström, G. *J. Phys. Chem.* **1994**, *98*, 8224–8233.
(73) Kokubo, H.; Pettitt, B. M. *J. Phys. Chem. B* **2007**, *111*, 5233–5242.
(74) Bernal, J. D.; Fowler, R. H. *J. Chem. Phys.* **1933**, *1*, 515–548.
(75) Robinson, D. R.; Jencks, W. P. *J. Am. Chem. Soc.* **1965**, *87*, 2462–2470.
(76) Lin, T.-Y.; Timasheff, S. N. *Biochemistry* **1994**, *33*, 12695–12701.
(77) Zou, Q.; Bennion, B. J.; Daggett, V.; Murphy, K. P. *J. Am. Chem. Soc.* **2002**, *124*, 1192–1202.
(78) Batchelor, J. D.; Olteanu, A.; Tripathy, A.; Pielak, G. J *J. Am. Chem. Soc.* **2004**, *126*, 1958–1961.
(79) Street, T. O.; Bolen, D. W.; Rose, G. D. *Proc. Natl. Acad. Sci. U.S.A.* **2006**, *103*, 13997–14002.
(80) Rösgen, J.; Pettitt, B. M.; Bolen, D. W. *Protein Sci.* **2007**, *16*, 733–743.
(81) Paul, S.; Patey, G. N. *J. Am. Chem. Soc.* **2007**, *129*, 4476–4482.

comes from the well-founded[8,16–19] assumption that the solute-induced perturbation is short-ranged, so that the measured effects, to an excellent approximation, can be attributed to the primary hydration shell.

The perturbation of water structure and dynamics by apolar molecular fragments has profound biological implications. The results presented here provide a "baseline" for studies of protein hydration dynamics at low temperatures. In particular, the peptides NAGMA and NALMA serve as models for unfolded proteins. For folded proteins, the intricate surface topography features solvent-penetrated pockets with more substantial perturbations of water dynamics than at the convex parts of the surface.[83,84]

Acknowledgment. We thank Torbjörn Drakenberg, Hans Lilja, and Erik Persson for helpful advice and the Swedish Research Council for financial support.

Supporting Information Available: Full description of methods, control experiments, and calculation of hydration numbers, DHNs and DPFs. Tables S1−S4. This material is available free of charge via the Internet at http://pubs.acs.org.

JA802668W

(82) O'Brien, E. P.; Dima, R. I.; Brooks, B.; Thirumalai, D. *J. Am. Chem. Soc.* **2007**, *129*, 7346–7353.
(83) Modig, K.; Liepinsh, E.; Otting, G.; Halle, B. *J. Am. Chem. Soc.* **2004**, *126*, 102–114.
(84) Halle, B. *Philos. Trans. R. Soc. London, Ser. B* **2004**, *359*, 1207–1224.

Supporting Information

Thermal signature of hydrophobic hydration dynamics

Johan Qvist and Bertil Halle

Contribution from the Department of Biophysical Chemistry,
Center for Molecular Protein Science, Lund University, SE-22100 Lund, Sweden

S1. Water/Heptane Partitioning

The use of the emulsion technique[1] for studies of supercooled aqueous solutions rests on the assumption that the chemical composition of the aqueous emulsion droplets is the same as in the aqueous solution from which the emulsion was prepared. In our case, this requires (*i*) that the mutual solubilities of water and *n*-heptane are negligibly small in the temperature range 243 – 268 K and (*ii*) that the solubilities of the four hydrophobic solutes in *n*-heptane are negligibly small in this temperature range. At 273 K, the solubility of *n*-heptane in water is 44 μM.[2] Even if the solubility increases somewhat at lower temperatures, it remains 3 orders of magnitude smaller than the solute concentrations used in our ^{2}H relaxation experiments. At 273 K, the solubility of water in *n*-heptane is 1 mM,[2] decreasing at lower temperatures. Consequently, less than one in 55000 water molecules in the emulsion sample are located in the heptane phase and the relative reduction of N_W is less than 20 ppm.

The partitioning of each of the four solutes between water and *n*-heptane was examined by ^{1}H NMR spectroscopy using maleic acid as internal standard. The gravimetrically determined concentration C_0 of the investigated D_2O solutions of these solutes are given in Table S1. The known amounts of solute and D_2O yield the water/solute mole ratio N_W (used for the analysis of the ^{2}H relaxation data). To obtain C_0, we also need the partial specific volumes of the solutes: 0.83 cm^3 g^{-1} for NAGMA, 0.93 cm^3 g^{-1} for NALMA,[3] 0.97 cm^3 g^{-1} for TMAO,[4] and 0.99 cm^3 g^{-1} for TMU[5] (all at 298 K). 300 μl of each of these solutions was mixed with an equal volume of a D_2O solution of maleic acid of known concentration, whereupon pH* was adjusted to 4.5 by addition of 4 μL 10 M NaOH. The solute concentration was then determined by comparing the integrated intensities of the solute CH_3 and maleic acid CH peaks. The ^{1}H spectra were acquired at 500 MHz on a Varian VnmrS DirectDrive spectrometer, using a 90° pulse length of 6 μs and a

repetition time of 30 s (to allow for the slow relaxation of methyl protons). The carrier frequency was set midway between the CH and CH_3 resonances to achieve equal excitation of the two peaks. The NMR-derived solute concentration C_{NMR}^{298}(aq) agreed within 1 % with the gravimetrically determined (nominal) concentration C_0, except for TMAO where it was 3 % lower (Table S1), consistent with the lower purity stated by the manufacturer.

To mimic conditions in the emulsion, the solution containing hydrophobic solute and maleic acid was mixed with an equal volume *n*-heptane and phase transfer equilibrium was established by vigorous shaking for at least 4 h. At pH* 4.5, one of the carboxyl groups of maleic acid is ionized (pK_{a1} = 1.92, pK_{a2} = 6.23) so migration of the internal standard into the heptane phase can safely be neglected. The solution was allowed to phase separate overnight, whereupon a ^{1}H NMR spectrum was acquired on the aqueous phase. The resulting solute concentration C_{NMR}^{298}(em) was not significantly different from the one determined before heptane partitioning (Table S1). The procedure was repeated at 278 K, with the same result (Table S1). We thus conclude that the concentrations (and N_W values) of the four investigated solutes are not significantly affected by incorporation into emulsion droplets.

Table S1. Concentration of samples determined gravimetrically and by ^{1}H NMR with (em) or without (aq) prior water/heptane partitioning at 298 or 278 K.

Solute	C_0 (mM)	C_{NMR}^{298}(aq)/C_0	C_{NMR}^{298}(em)/C_0	C_{NMR}^{278}(em)/C_0
NAGMA	58.9	0.997	1.005	1.013
NAGMA	216.3	0.990	0.996	0.988
NALMA	50.0	0.997	0.985	0.991
NALMA	192.3	0.994	1.008	0.990
TMAO	75.0	0.969	0.965	0.970
TMAO	207.8	0.971	0.972	0.975
TMU	52.9	–	1.013	1.000
TMU	194.2	–	1.030	1.042

S2. Water ^{2}H and ^{17}O Control Experiments

To check the assumptions made in the analysis of the water ^{2}H relaxation data, several control experiments were carried out at 288 K. Table S2 presents four sets of relative relaxation enhancements $(R_1 - R_1^0)/R_1^0$, determined in these experiments with an estimated accuracy of ±0.008 (based on 0.5 % accuracy in T_1).

From the first two sets, we conclude that incorporation of the aqueous solution in emulsion droplets has no significant effect on the water ^{2}H relaxation. This finding is consistent with the preceding demonstration that the chemical composition of the aqueous phase is unaffected by the *n*-heptane phase in the emulsion. Moreover, it shows that hydration of the droplet interface does not affect R_1 significantly. This is as expected since only one in ~ 5000 water molecules is in contact with the interface of a droplet with 10 μm diameter.

From the second and third data sets, we conclude that there is no significant frequency dependence in R_1 at the high frequencies used here. In other words, we are in the extreme motional narrowing regime, where R_1 is proportional to the time integral of the orientational time correlation function.[6] [At low frequencies, below 1 MHz, a frequency dependence in water ^{2}H R_1 from emulsion samples has been observed and tentatively attributed to droplet shape fluctuations (C. Mattea, unpublished results).]

The third and fourth data sets compare ^{2}H and ^{17}O relaxation data acquired on the same D_2O solutions (with ^{17}O at natural abundance). In the present samples, the ^{2}H and ^{17}O relative relaxation enhancements might differ for two reasons. Labile solute deuterons exchanging rapidly with water deuterons can substantially increase the ^{2}H enhancement, but cannot affect ^{17}O relaxation. While NAGMA and NALMA each carries two labile amide N–D deuterons, they are in the slow-exchange regime at pH* 4.5.[7] Consistent with this expectation, there is no significant difference between the ^{2}H and ^{17}O enhancements for NAGMA or NALMA. (For alcohols, on the other hand, the hydroxyl deuteron exchanges at a higher rate and may contribute significantly to the ^{2}H relaxation.[8-11]) The second potential source of a ^{2}H/^{17}O difference is anisotropic water reorientation, which presumably accounts for the significantly smaller ^{17}O enhancements for TMAO and TMU (Table S2). That a difference is observed only for the two most hydrophobic solutes suggests that the anisotropy is associated with the nonpolar part of the hydration shell.

Table S2. Relative water ^{2}H or ^{17}O relaxation enhancement at 288 K in solution and emulsion samples and at different resonance frequencies.

		$(R_1 - R_1^0)/R_1^0$			
		Solution	Emulsion	Emulsion	Emulsion
Solute	C_0 (mM)	^{2}H, 55.5 MHz	^{2}H, 55.5 MHz	^{2}H, 76.8 MHz	^{17}O, 67.8 MHz
NAGMA	216.3	0.052	0.062	0.056	0.053
NALMA	192.3	0.130	0.123	0.128	0.135
TMAO	207.8	0.065	0.066	0.068	0.046
TMU	194.2	0.081	0.084	0.082	0.050

S3. Hydration Numbers from MD simulations and SASA Calculations

Molecular dynamics simulations were performed with the AMBER code. Geometrical and Lennard-Jones parameters for the solutes were obtained from the General Amber Force Field[12] and partial atomic charges were determined with the AM1-BCC method[13] (NAGMA, NALMA and TMU) or taken from a previous study[14] (TMAO). The rectangular simulation box was filled with SPCE water[15] to obtain solute concentrations of ~ 35 mM (Table S3). After energy minimization and equilibration, the MD simulation was performed at 300 K and 1 atm with periodic boundary conditions, particle-mesh Ewald summation for long-range electrostatics, 12 Å cutoff for nonbonded interactions, constrained X–H bonds, and 2 fs time step. Atomic coordinates were saved every 1 ps of the 1 ns trajectory. No significant drift in energy, temperature or density was observed.

The 1000 MD configurations were used to compute the hydration number ν_H (Table S3), defined as the mean number of water molecules satisfying at least one of the following geometric criteria: $R(O_W–O) < 3.3$ Å, $R(O_W–N) < 3.5$ Å and $R(O_W–C) < 5.0$ Å. The C cutoff is close to the (broad and shallow) first minimum in the O_W–C radial distribution function for aliphatic carbons.[16-19] The O and N cutoffs are also close to typical radial distribution function minima, but

Table S3. Hydration numbers and solvent-accessible surface areas for four solutes.

Solute	N_W	C (mM)	ν_H	A_S	a_W
NAGMA	1631	33.8	33.3	361.8	10.87
NALMA	1858	29.6	42.6	454.0	10.65
TMAO	1422	38.8	25.1	270.1	10.75
TMU	1483	37.2	32.0	342.5	10.71

their values are less important. (For the four solutes examined here, the O and N cutoffs can be increased by 0.5 Å without affecting ν_H.) We also performed a 1 ns MD simulation of a 37.4 mM benzene solution, obtaining $\nu_H = 26.7$ for $R(O_W–C) < 5.0$ Å. This ν_H value falls between the hydration numbers 23 [20] and 31 [21] reported previously for benzene.

To compute a consistent set of hydration numbers for the large number of solutes for which water ^{17}O or ^{2}H NMR relaxation data have been reported, we used the relation

$$\nu_H = \frac{A_S}{a_W} \qquad \text{(S1)}$$

The solvent-accessible surface area A_S was computed with GetArea 1.1,[22] using the following standard set of united-atom van der Waals radii: R(C3H0) = 1.70 Å, R(C3H1) = 1.85 Å, R(C4Hn) = 2.00 Å, R(N3H0) = 1.50 Å, R(N3H1) = 1.70 Å, R(N3H2) = 1.80 Å, R(N4H3) = 2.00 Å, R(O1H0) = 1.40 Å and R(O2H1) = 1.50 Å. Here XnHm denotes an atom of element X with n bonds and m attached H atoms. The probe radius $R_{probe} = 1.7$ Å was chosen so that $R(X) + R_{probe}$ is close to the first maximum in the radial distribution function. Note that A_S only depends on the sum $R(X) + R_{probe}$. In eq (S1), a_W is the amount of solvent-accessible area occupied by one water molecule on average. Its value was fixed at 10.75 Å, the average a_W value for the four solutes required to reproduce the MD-derived ν_H values with eq (S1) (Table S3). Hydration numbers ν_H computed in this way are given for 40 solutes in Table S4.

Table S4. Hydration dynamics parameters for 40 organic solutes at 298 K, derived from water ^{2}H or ^{17}O NMR relaxation data and computed hydration numbers.

Solute	ν_H	ν_{dyn}	ξ	Solvent	Ref.
methanol	17.2	5.8	1.34	H_2O	[23]
ethanol	20.4	10.5	1.51	H_2O	[23]
n-propanol	23.3	14.1	1.60	H_2O	[23]
i-propanol	23.2	16.4	1.71	H_2O	[23]
n-butanol	26.2	17.1	1.65	H_2O	[23]
t-butanol	25.6	22.7	1.89	H_2O	[23]
n-pentanol	29.1	19.4	1.67	H_2O	[23]
1,2-ethanediol	21.5	5.7	1.27	H_2O	[23]
1,3-propanediol	24.4	10.3	1.42	H_2O	[23]
1,4-butanediol	27.3	14.0	1.51	H_2O	[23]
1,5-pentanediol	30.2	18.4	1.61	H_2O	[23]
2-amino-ethanol	22.3	8.4	1.38	H_2O	[24]
3-amino-*n*-propanol	25.4	13.9	1.55	H_2O	[24]
4-amino-*n*-butanol	28.3	16.8	1.59	H_2O	[24]
5-amino-*n*-pentanol	31.2	23.2	1.74	H_2O	[24]
formamide	17.8	–0.1 ± 0.3	0.99 ± 0.02	H_2O	[25]
N-methyl-formamide	21.4	4.3 ± 0.3	1.20 ± 0.02	H_2O	[25]
N-ethyl-formamide	24.5	8.0 ± 0.3	1.33 ± 0.01	H_2O	[25]
N,N'-dimethyl-formamide	24.7	8.2 ± 0.3	1.33 ± 0.01	H_2O	[25]
acetamide	21.7	4.7 ± 0.3	1.22 ± 0.02	H_2O	[25]
N-methyl-acetamide	25.0	9.9 ± 0.3	1.40 ± 0.01	H_2O	[25]
N-ethyl-acetamide	28.1	15.1 ± 0.4	1.54 ± 0.01	H_2O	[25]
N-*n*-propyl-acetamide	31.0	16.4 ± 0.4	1.53 ± 0.01	H_2O	[25]

Table S4. Continued.

Solute	ν_H	ν_{dyn}	ξ	Solvent	Ref.
N-*n*-butyl-acetamide	33.9	19.8 ± 0.4	1.58 ± 0.01	H_2O	[25]
N-methyl-*n*-propamide	27.7	14.5 ± 0.4	1.52 ± 0.01	H_2O	[25]
N-methyl-*n*-butamide	30.6	18.4 ± 0.4	1.60 ± 0.01	H_2O	[25]
urea	20.6	–0.1 ± 0.3	1.00 ± 0.02	H_2O	[26]
methylurea	23.8	7.4 ± 0.4	1.31 ± 0.02	H_2O	[26]
N,N-dimethylurea	26.4	10.1 ± 0.2	1.38 ± 0.01	H_2O	[26]
N,N'-dimethylurea	27.1	12.4 ± 0.2	1.46 ± 0.01	H_2O	[26]
tetramethylurea	32.0	19.4 ± 0.2	1.61 ± 0.01	H_2O	[26]
tetramethylurea	32.0	19.1 ± 2.0	1.60 ± 0.06	D_2O	[a]
trimethylamine N-oxide	25.1	16.6 ± 1.9	1.66 ± 0.07	D_2O	[a]
glycine	23.4	3.9	1.17	H_2O	[27]
alanine	25.9	10.7	1.41	H_2O	[27]
valine	30.1	20.1	1.67	H_2O	[27]
leucine	33.0	26.6	1.81	H_2O	[27]
isoleucine	32.6	19.0	1.58	H_2O	[27]
diglycine	32.0	8.9	1.28	H_2O	[27]
NAGMA	33.3	14.4 ± 1.8	1.43 ± 0.05	D_2O	[a]
NALMA	42.6	30.8 ± 2.1	1.72 ± 0.05	D_2O	[a]

[a] This work.

References

(1) Rasmussen, D. H.; MacKenzie, A. P. *J. Chem. Phys.* **1973**, *59*, 5003–5013.

(2) Polak, J.; Lu, B. C.-Y. *Can. J. Chem.* **1973**, *51*, 4018–4023.

(3) Liu, J. L.; Hakin, A. W.; Hedwig, G. R. *J. Sol. Chem.* **2001**, *30*, 861–883.

(4) Lin, T.-Y.; Timasheff, S. N. *Biochemistry* **1994**, *33*, 12695–12701.

(5) Philip, P. R.; Perron, G.; Desnoyers, J. E. *Can. J. Chem.* **1974**, *52*, 1709–1713.

(6) Abragam, A. *The Principles of Nuclear Magnetism*; Clarendon Press: Oxford, 1961.

(7) Bai, Y.; Milne, J. S.; Mayne, L.; Englander, S. W. *Proteins* **2004**, *17*, 75–86.

(8) Goldammer, E. v.; Hertz, H. G. *J. Phys. Chem.* **1970**, *74*, 3734–3755.

(9) Nakahara, M.; Yoshimoto, Y. *J. Phys. Chem.* **1995**, *99*, 10698–10700.

(10) Seto, T.; Mashimo, T.; Yoshiya, I.; Shimizu, A.; Fumino, K.; Taniguchi, Y. *J. Mol. Liq.* **1996**, *70*, 1–9.

(11) Yoshida, S.; Ibuki, K.; Ueno, M. *J. Chem. Phys.* **1998**, *108*, 1360–1367.

(12) Wang, J.; Wolf, R. M.; Caldwell, J. W.; Kollman, P. A.; Case, D. A. *J. Comput. Chem.* **2004**, *25*, 1157–1174.

(13) Jakalian, A.; Jack, D. B.; Bayly, C. I. *J. Comput. Chem.* **2002**, *23*, 1623–1641.

(14) Kast, K. M.; Brickmann, J.; Kast, S. M.; Berry, R. S. *J. Phys. Chem. A* **2003**, *107*, 5342–5351.

(15) Berendsen, H. J. C.; Grigera, J. R.; Straatsma, T. P. *J. Phys. Chem.* **1987**, *91*, 6269–6271.

(16) Vaisman, I. I.; Brown, F. K.; Tropsha, A. *J. Phys. Chem.* **1994**, *98*, 5559–5564.

(17) Meng, E. C.; Kollman, P. A. *J. Phys. Chem.* **1996**, *100*, 11460–11470.

(18) Bridgeman, C. H.; Buckingham, A. D.; Skipper, N. T. *Chem. Phys. Lett.* **1996**, *253*, 209–215.

(19) Kalko, S. G.; Guàrdia, E.; Padró, J. A. *J. Phys. Chem. B* **1999**, *103*, 3935–3941.

(20) Linse, P. *J. Am. Chem. Soc.* **1990**, *112*, 1744–1750.

(21) Raschke, T. M.; Levitt, M. *Proc. Natl. Acad. Sci. USA* **2005**, *102*, 6777–6782.

(22) Fraczkiewicz, R.; Braun, W. *J. Comput. Chem.* **1998**, *19*, 319–333.

(23) Ishihara, Y.; Okouchi, S.; Uedaira, H. *J. Chem. Soc., Faraday Trans.* **1997**, *93*, 3337–3342.

(24) Okouchi, S.; Tsuchida, K.; Yoshida, S.; Ishihara, Y.; Ikeda, S.; Uedaira, H. *Bull. Chem. Soc. Jpn.* **2005**, *78*, 424–429.

(25) Bagno, A.; Lovato, G.; Scorrano, G.; Wijnen, J. W. *J. Phys. Chem.* **1993**, *97*, 4601–4607.

(26) Shimizu, A.; Fumino, K.; Yukiyasu, K.; Taniguchi, Y. *J. Mol. Liq.* **2000**, *85*, 269–278.

(27) Ishimura, M.; Uedaira, H. *Bull. Chem. Soc. Jpn.* **1990**, *63*, 1–5.